The Journal of Engineering

*The 14th IET International Conference on AC and DC Power Transmission (ACDC 2018)*

IET Journals
The Institution of Engineering and Technology

# Stability analysis of grid-connected PV generation with an adapted reactive power control strategy

eISSN 2051-3305
Received on 23rd August 2018
Accepted on 19th September 2018
E-First on 7th December 2018
doi: 10.1049/joe.2018.8485
www.ietdl.org

*Gangui Yan[1], Yuru Cai[1] ✉, Qi Jia[1], Shuai Liang[1]*

[1]*College of Electrical Engineering, Northeast Electric Power University, Jilin, Jilin, People's Republic of China*

✉ *E-mail: sxyccyr@163.com*

**Abstract:** The static VAR compensator is widely applied in large-scale grid-connected photovoltaic (PV) generation to participate in voltage regulation of power system, which ignores the reactive power regulation capability of PV inverter. In this study, firstly, the constraints of maximum operating current and output voltage's amplitude of PV inverter are considered, and the reactive power regulation capability of the PV generation is evaluated; secondly, an active participation in voltage regulation and control strategy of PV generation is proposed considering reactive power demand of system. This control method through the real-time detection and comparison with reference value of point of common coupling (PCC) voltage, automatically obtain the reactive demand to maintain PCC voltage by PI controller and realises the dynamic adjustment; finally, a time-domain small-signal model for PV generation is established, and based on this small-signal model, eigenvalue analysis is employed to study the influence of the grid strength, operating condition, and the reactive power control strategy on operating stability. Based on the time-domain simulation example in EMTDC/PSCAD, the validity of the theoretical analysis and the feasibility of the control strategy are verified.

## 1 Introduction

Benefiting from the significant technical advances in solar cells and power electronics, the penetration of large-scale photovoltaic (PV) generation is increasing year by year. Due to the low energy densities and uneven distributions of solar resources, most PV power plants are deployed in remote areas or even desert with high solar irradiance [1]. Consequently, the long-distance power transmission lines with low short circuit ratio (SCR) have become the major bottleneck to effectively transmit the generated power to the load centre [2]. Due to the perturbation of the PV array output power and the disturbance of the power grid and other aspects, the point of common coupling (PCC) voltage fluctuates easily [3], even worse when connect to weak grid. Large-scale PV generation affects the power flow sise and distribution of transmission side grid [4], therefore, large-scale grid-connected PV generation should have ability to regulate reactive power and participate in voltage control of grid according to the PCC voltage, so as to meet the reactive power demand of grid.

To unblock the bottleneck caused by PCC voltage fluctuation, the scholars have done quite a lot of work and got tremendous analyse result on this field. Liu *et al*. [5] show that the voltage regulation capacity of PV generation can completely replace the voltage regulator capacitor when penetration is >30%. Alam *et al*. [6] designed two kinds of voltage source converter (VSC) reactive power control modes, by using fuzzy adaptive control strategy to support grid voltage when PV output or load fluctuated. Research on voltage control for PV generation in China is mostly focused on distributed generation [7, 8]. Jahangiri and Aliprantis [7] utilised energy storage for voltage regulation, which could suppress active fluctuation but increased the cost and complicates the control system. [8] mainly utilised reactive compensation for local load, but could not realise the reactive power independent control of the PV generation.

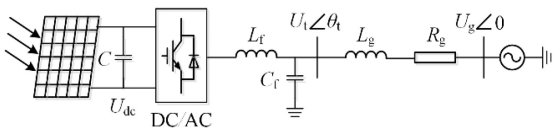


**Fig. 1** *PV generation access weak grid structure*

In summary, existing researches mostly focus on distributed generation, lack of research on active participating voltage regulation of large-scale PV generation.

In this paper, firstly, the constraints of maximum operating current and output voltage's amplitude of PV inverter are considered, and the reactive power regulation capability of the PV generation is evaluated. Secondly, an active participation in voltage regulation and control strategy of PV generation is proposed considering reactive power demand of system. Finally, a time-domain small-signal model for PV generation is established, and based on this small-signal model, eigenvalue analysis is employed to study the influence of the grid strength and the reactive power control strategy on operating stability. Based on the time-domain simulation example in EMTDC/PSCAD, the validity of the theoretical analysis and the feasibility of the control strategy are verified.

## 2 Main structure and control strategy

### 2.1 Main structure of the system

In this paper, a single PV unit connected to an infinity system is used to equivalent the discussing system. The structure of PV generation through VSC connected to AC grid is shown in Fig. 1. $C$ is DC filter capacitor, $U_{DC}$ is DC voltage, $L_f$ is filter inductance of inverter, $C_f$ is filter capacitor of VSC, $R_g$ and $L_g$ are resistance and inductance of grid, $U_t$ and $U_g$ are the PCC voltage and grid voltage.

In Fig. 1, the AC grid strength is generally described by the short SCR, which is the ratio of the short circuit capacity of the AC system to the rated power of the PV generation. As shown in (1)

$$\mathrm{SCR} = \frac{S_{AC}}{P_N} = \frac{U_N^2}{Z_g \cdot P_N} \tag{1}$$

where $Z_g$ is the grid resistance, $U_N$ is the rating of the grid line voltage. Weak AC system usually refers to the AC system operating at $2 \le \mathrm{SCR} \le 3$.

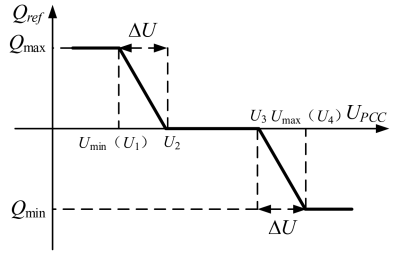


**Fig. 2** *Topology of VSC*

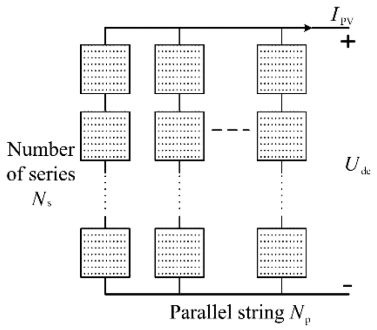


**Fig. 3** *PV cell equivalent circuit*

### *2.2 Analysis of the limit of reactive power regulation*

The function of reactive power regulation on improving system operation voltage level is apparently, especially connected to weak AC system. The VSC can provide active power and reactive power to system simultaneously, for maintaining PCC voltage constantly.

The reactive power generated by VSC is mainly restricted by the following factors:

i. The margin of $I_{max}$ maximum operating current $I_{max}$ usually takes 10% of the rated current value, in order to ensure the operation safety of VSC. So the amplitude of $I_{max}$ is $\sqrt{2} * 1.1 I_N$.
ii. As for a three-phase inverter circuit using SPWM (sinusoide pulse width modulation), the range of modulation ratio $m$ is (0, 1] to ensure the effectiveness of SPWM control and waveform quality of output voltage of VSC. When modulation ratio is 1, the fundamental wave amplitude of the output phase voltage is $U_{dc}/2$ maximum.

The main parameters are discussed as follows, $S_N$, $U_N$, and $I_N$ are rated capacity, voltage, and current, $L$ is a filter reactance, $U_{dc}$ is DC busbar voltage, $U_{PCC}$ is voltage of PCC.

According to the main operation constraints of VSC, the reactive power regulation capability is analysed. The maximum current constraint conditions can be obtained by (2).

$$I_d^2 + I_q^2 \le I_{max}^2 \tag{2}$$

The active power and reactive power of VSC are as (3).

$$\begin{cases} P = U_d \cdot i_d \\ Q = -U_d \cdot i_q \end{cases} \tag{3}$$

Equation (3) is brought into (2) and can be obtained:

$$-\sqrt{U_{PCC}^2 I_{max}^2 - P^2} \le Q \le \sqrt{U_{PCC}^2 I_{max}^2 - P^2} \tag{4}$$

The maximum voltage constraint conditions can be obtained in (5).

$$U_d^2 + U_q^2 \le \frac{1}{4} U_{DC}^2 \tag{5}$$

Derived from (6).

$$-\sqrt{\left(\frac{U_{DC}U_{PCC}}{2\omega L}\right)^2 - P^2} - \frac{U_{PCC}^2}{\omega L} \le Q \le \sqrt{\left(\frac{U_{DC}U_{PCC}}{2\omega L}\right)^2 - P^2} - \frac{U_{PCC}^2}{\omega L} \tag{6}$$

The lower limit of reactive power regulation is $Q_{min}$, and the upper limit of reactive power regulation is $Q_{max}$.

$$\begin{aligned} Q_{min} &= \min\left\{-\sqrt{\left(\frac{U_{DC}U_{PCC}}{2\omega L}\right)^2 - P^2} - \frac{U_{PCC}^2}{\omega L}, \quad -\sqrt{u_{PCC}^2 I_{max}^2 - P^2}\right\} \\ Q_{max} &= \max\left\{\sqrt{\left(\frac{U_{DC}U_{PCC}}{2\omega L}\right)^2 - P^2} - \frac{U_{PCC}^2}{\omega L}, \quad \sqrt{u_{PCC}^2 I_{max}^2 - P^2}\right\} \end{aligned} \tag{7}$$

### *2.3 Adapted reactive power control strategy*

Based on the constraints mentioned above, an active participation in voltage regulation and control strategy of PV generation is proposed considering reactive power demand of system. This control method through the real-time detection and comparison with reference value of PCC voltage, automatically obtain the reactive demand to maintain PCC voltage by PI controller and realises the dynamic adjustment.

These strategy provide the opportunity to keep $Q_{ref} = 0$ when the voltage is within an acceptable boundary. Fig. 2 illustrates Specific control; however, $U$min and $U$max are different for each voltage. Using this method, the maximum capacity of the VSC is demanded for reactive power support when $U_{PCC} \le U_{min}$ or $U_{PCC} \ge U_{max}$; however, the support will be fully provided only if the other voltage is $(U_{min} + \Delta U) \le U_{PCC} \le (U_{max} - \Delta U)$.

The expression equations of the control strategy are as (8).

$$Q_{ref} = \begin{cases} Q_{max} & U_{PCC} \le U_1 \\ \dfrac{Q_{max}}{U_1 - U_2}(U_{PCC} - U_1) & U_1 < U_{PCC} \le U_2 \\ 0 & U_2 < U_{PCC} \le U_3 \\ \dfrac{Q_{max}}{U_3 - U_4}(U_{PCC} - U_3) & U_3 < U_{PCC} \le U_4 \\ -Q_{max} & U_{PCC} > U_4 \end{cases} \tag{8}$$

## 3 Small-signal modelling

### *3.1 PV array modeling*

PV array composed of a parallel string of $N_s$, which formed by $N_p$ PV cells is shown in Fig. 3, where $U_{DC}$ and $I_{PV}$ are output voltage and current of PV array.

Based on the consistency of the operating characteristics of the PV cells, the $U_{DC}$–$I_{PV}$ of PV array port can be obtained by (9).

$$I_{PV} = N_P I_{SC}\left[1 - C_1\left(e^{(U_{DC})/C_2 N_s U_{OC}} - 1\right)\right] \tag{9}$$

where $I_{sc}$ is short-circuit current, $U_{oc}$ is open-circuit voltage, $C_1$ and $C_2$ are constant.

### *3.2 Model of the VSC and the control system*

Configuration of VSC as shown in Fig. 4. The model of VSC in $dq$ frame is shown in (10).

$$\begin{cases} L\dfrac{di_d}{dt} = U_d - U_{td} + \omega L i_q \\ L\dfrac{di_q}{dt} = U_q - U_{tq} + \omega L i_q \\ U_{DC} \cdot C\dfrac{dU_{DC}}{dt} = i_{PV} \cdot U_{DC} - U_{td} \cdot i_d \end{cases} \tag{10}$$

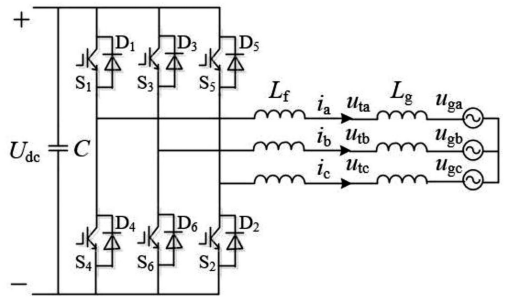


**Fig. 4** *Topology of VSC*

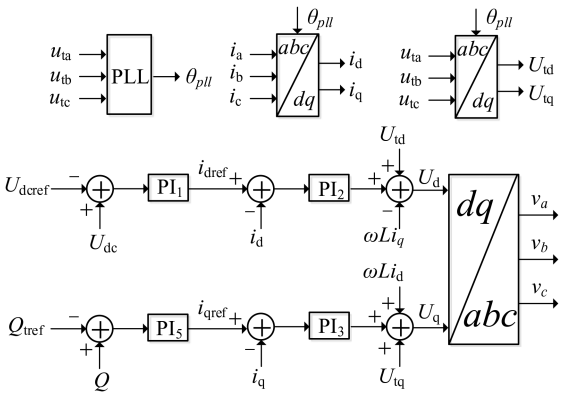


**Fig. 5** *Control strategy of VSC*

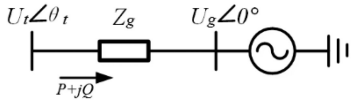


**Fig. 6** *PV generation access weak grid structure*

The vector control strategy based on grid voltage orientation is often used in VSC control, as shown in Fig. 5. The current command values of the $d$-axis and the $q$-axis are generated, respectively, according to the demand of active power and reactive power controlled by the power outer loop. The constant DC voltage control mode is applied to the control of active power while the constant terminal voltage amplitude control method is applied to the reactive power control. Where $U_{\mathrm{DCref}}$ and $U_{\mathrm{DC}}$ are reference value and actual value of DC voltage.

The governing equation of the control strategy of the VSC in Fig. 5 as follows: (see (11)) where $x_1$, $x_2$, $x_3$ and $x_5$ are state varables; $k_{\mathrm{p1}}$, $k_{\mathrm{p2}}$, $k_{\mathrm{p3}}$, $k_{\mathrm{p4}}$ and $k_{\mathrm{p5}}$ are the proportional coefficients of the controllers; $k_{\mathrm{i1}}$, $k_{\mathrm{i2}}$, $k_{\mathrm{i3}}$, $k_{\mathrm{i4}}$ and $k_{\mathrm{i5}}$ are the integral coefficients of the controllers; $\theta_{\mathrm{pll}}$ is the angle produced by the phase-locked loop.

### 3.3 Model of PV generation connected to grid

The equivalent circuit of AC side of PV generation connected to AC system is shown in Fig. 6, where $P$ and $Q$ are the active power and reactive power.

According to the circuit principle

$$U_{tx} + jU_{ty} = U_{gx} + jU_{gy} + j(i_x + ji_y)x_g \tag{12}$$

The grid connection point voltage of VSC and the $xy$ axis component of grid-connected current, $U_{tx}$, $U_{ty}$, $i_x$, $i_y$ and $dq$ axis component $U_{td}$, $U_{tq}$, $i_d$, $i_q$ satisfy the following relationships.

$$\begin{cases} U_{tx} = U_{td} \cdot \cos\theta_{\mathrm{pll}} - U_{tq} \cdot \sin\theta_{\mathrm{pll}} \\ U_{ty} = U_{td} \cdot \sin\theta_{\mathrm{pll}} + U_{tq} \cdot \cos\theta_{\mathrm{pll}} \\ i_x = i_d \cdot \cos\theta_{\mathrm{pll}} - i_q \cdot \sin\theta_{\mathrm{pll}} \\ i_y = i_d \cdot \sin\theta_{\mathrm{pll}} + i_q \cdot \cos\theta_{\mathrm{pll}} \end{cases} \tag{13}$$

In summary, (9)–(13) compose the differential equations of PV generation, the equations are linearised at the equilibrium point to get the small-signal model of PV generation connected to AC system.

Status variables $\Delta x$ are selected as follow:

$$\Delta x = \left[\Delta x_1, \Delta x_2, \Delta x_3, \Delta x_5, \Delta x_{\mathrm{pll}}, \Delta\theta_{\mathrm{pll}}, \Delta i_d, \Delta i_q, \Delta U_{\mathrm{DC}}\right]^T$$

## 4 Eigenvalues analysis

Taking the PV generation shown in Fig. 1 as an example to analysis the small-signal stability, the main parameters of the system are summarised in Table 1, when SCR = 1.5, the eigenvalues of the system state matrix are summarised in Table 2. Fig. 7 shows that all the eigenvalues of the system are distributed on the left side of the complex plane, and the PV generation is connected to weak grid with small disturbance stability. There are five attenuation modes and two oscillation modes in the system.

Considering the influence of grid strength, reactive power control parameters and reactive loop parameters on small-signal stability of PV generation, the change regulation of the characteristic root is mainly analysed.

The eigenvalues locus for SCR varies from 4.5 to 1.5 is shown in Fig. 8. As the grid strength decreases, it can be seen that there are five eigenvalues changing $\lambda_1$, $\lambda_5$, $\lambda_6$ move to right-half plane; $\lambda_3$, $\lambda_4$ move to right-half plane. Therefore, the stability of the PV generation connected to weak grid becomes worse with reduction of grid strength.

As the absolute value of reactive power control parameter $k$ increase, it can be seen from Fig. 9 that there are five eigenvalues changing. $\lambda_1$, $\lambda_5$ and $\lambda_6$ move to left-half plane; $\lambda_3$, $\lambda_4$ move to right-half plane. Therefore, the stability of the PV generation becomes better with the absolute value of reactive power control parameter increasing.

$$\begin{cases} \dfrac{\mathrm{d}x_1}{\mathrm{d}t} = U_{\mathrm{DC}} - U_{\mathrm{DCref}} \\ \dfrac{\mathrm{d}x_2}{\mathrm{d}t} = k_{\mathrm{p1}} \cdot (U_{\mathrm{DC}} - U_{\mathrm{DCref}}) + k_{\mathrm{i1}} \cdot x_1 - i_d \\ \dfrac{\mathrm{d}x_3}{\mathrm{d}t} = k_{\mathrm{p5}} \cdot \left(-U_{td} \cdot i_q - (k \cdot U_t + b)\right) + k_{\mathrm{i5}} \cdot x_5 - i_q \\ \dfrac{\mathrm{d}x_5}{\mathrm{d}t} = Q - Q_{\mathrm{ref}} = -U_{td} \cdot i_q - (k \cdot U_t + b) \\ \dfrac{\mathrm{d}x_{\mathrm{pll}}}{\mathrm{d}t} = U_{tq} \\ \dfrac{\mathrm{d}\theta_{\mathrm{pll}}}{\mathrm{d}t} = k_{\mathrm{p4}} \cdot U_{tq} + k_{\mathrm{i4}} \cdot x_{\mathrm{pll}} + \omega_0 \\ U_d = k_{\mathrm{p2}}\left[k_{\mathrm{p1}}(U_{\mathrm{DC}} - U_{\mathrm{DCref}}) + k_{\mathrm{i1}} \cdot x_1 - i_d\right] + k_{\mathrm{i2}} \cdot x_2 + U_{td} - \omega L i_q \\ U_q = k_{\mathrm{p3}}\left[k_{\mathrm{p5}}\left(-U_{\mathrm{DC}} \cdot i_q - (k \cdot U_t + b)\right) + k_{\mathrm{i5}} \cdot x_5 - i_q\right] + k_{\mathrm{i3}} \cdot x_3 + U_{td} + \omega L i_d \end{cases} \tag{11}$$

**Table 1** Main parameters

| Parameter | Value |
|---|---|
| rated output power of PV generation $P$, kW | 500 |
| rated DC voltage $U_{DC}$, V | 600 |
| grid voltage $Ug$, V | 270 |
| DC filter capacitor $C$, F | 0.02 |
| inverter filter inductance $L_f$, mH | 0.5 |
| grid inductance $Lg$, mH | 0.3 |
| DC voltage control loop ($k_{p1}$, $k_{i1}$) | (2, 200) |
| AC voltage control loop ($k_{p5}$, $k_{i5}$) | (2, 100) |
| active current control loop ($k_{p2}$, $k_{i2}$) | (2, 100) |
| reactive current control loop ($k_{p3}$, $k_{i3}$) | (2, 100) |
| phase-locked loop ($k_{p4}$, $k_{i4}$) | (12, 1500) |

**Table 2** Eigenvalues of the system

| Mode | Eigenvalues | Oscillation frequency, Hz | Damping ratio |
|---|---|---|---|
| $\lambda_1$ | −1613835.6 | 0 | 1 |
| $\lambda_2$ | −3904.4 | 0 | 1 |
| $\lambda_{3,4}$ | −25.5 ± j71.9 | 11.4 | 0.33 |
| $\lambda_{5,6}$ | −3.2 ± j35.4 | 5.6 | 0.09 |
| $\lambda_7$ | −50.37 | 0 | 1 |
| $\lambda_8$ | −49.65 | 0 | 1 |
| $\lambda_9$ | −50.22 | 0 | 1 |

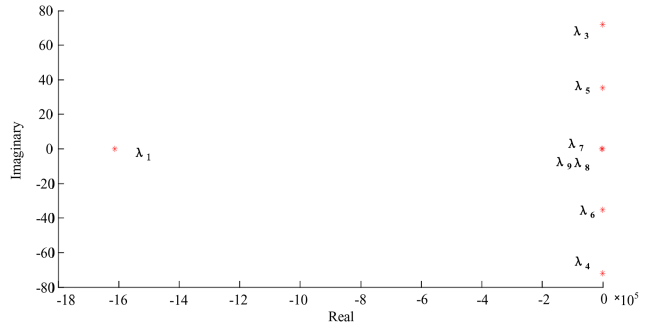


**Fig. 7** *Distribution of the characteristic root*

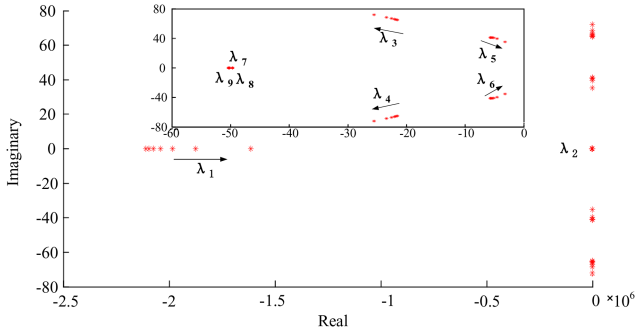


**Fig. 8** *Eigenvalues locus for varying grid strength*

When SCR = 4 and $k_{i5}$ = 100, only reactive loop proportional coefficient $k_{p5}$ changes (0.1–10), the root locus of system are shown as shown in Fig. 10. It can be seen that $\lambda_1$, $\lambda_5$ and $\lambda_6$ move to left-half plane; $\lambda_3$, $\lambda_4$ and $\lambda_9$ moves to right-half plane as the value of $k_{p5}$ increasing. Therefore, the increasing of $k_{p5}$ is good for system stability.

When SCR = 4 and $k_{p5}$ = 2, only reactive loop integral coefficient $k_{i5}$ changes (100–1000), the root locus of system are shown as shown in Fig. 11. It can be seen that $\lambda_5$, $\lambda_6$ and $\lambda_9$ move to left-half plane; $\lambda_3$, $\lambda_4$ move to right-half plane as the value of $k_{i5}$ increasing. Therefore, the increasing of $k_{i5}$ is good for system stability. There is no obvious change in dominant characteristic roots, which indicates that the parameters of the reactive loop have little effect on small-signal stability.

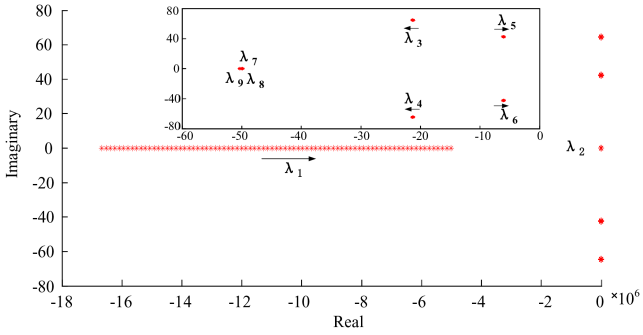


**Fig. 9** *Eigenvalues locus for varying control parameters (k)*

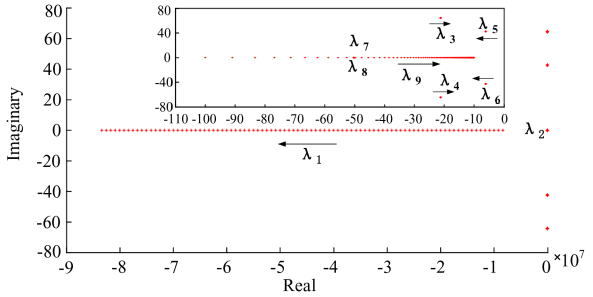


**Fig. 10** *Eigenvalues locus for varying reactive loop proportional coefficient ($k_{p5}$)*

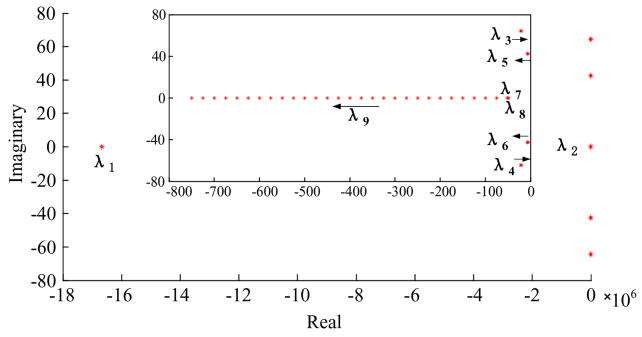


**Fig. 11** *Eigenvalues locus for varying reactive loop integral parameters ($k_{i5}$)*

## 5 Simulation validation

In order to verify the validity of the theoretical analysis and the feasibility of the control strategy, a time-domain simulation example is constructed in EMTDC/PSCAD as shown in Fig. 10. Due to the limitation of system capacity, the lower limit of reactive power regulation $Q_{min}$ and the upper limit of reactive power regulation $Q_{max}$ are −0.2 and 0.2 MVar. Other system simulation parameters are shown in Table 1.

### 5.1 Simulation of different reactive loop parameters

Fig. 12 shows the PCC voltage $U_{PCC}$, rated DC voltage $U_{DC}$, $q$-axis component current $i_q$ and output reactive power $Q_g$ when SCR = 4, $k_{p5}$ = 2, $k_{i5}$ = 100 at different values of reactive loop parameters (in Fig. 12*a* $k_{i5}$ = 100 and in Fig. 12*b* $k_{p5}$ = 2). From Fig. 12, PV generation faces grid disturbance at $t$ = 4 s which brings a damped oscillation, but final becomes stable. The larger value of reactive loop can make system back to a stable state faster.

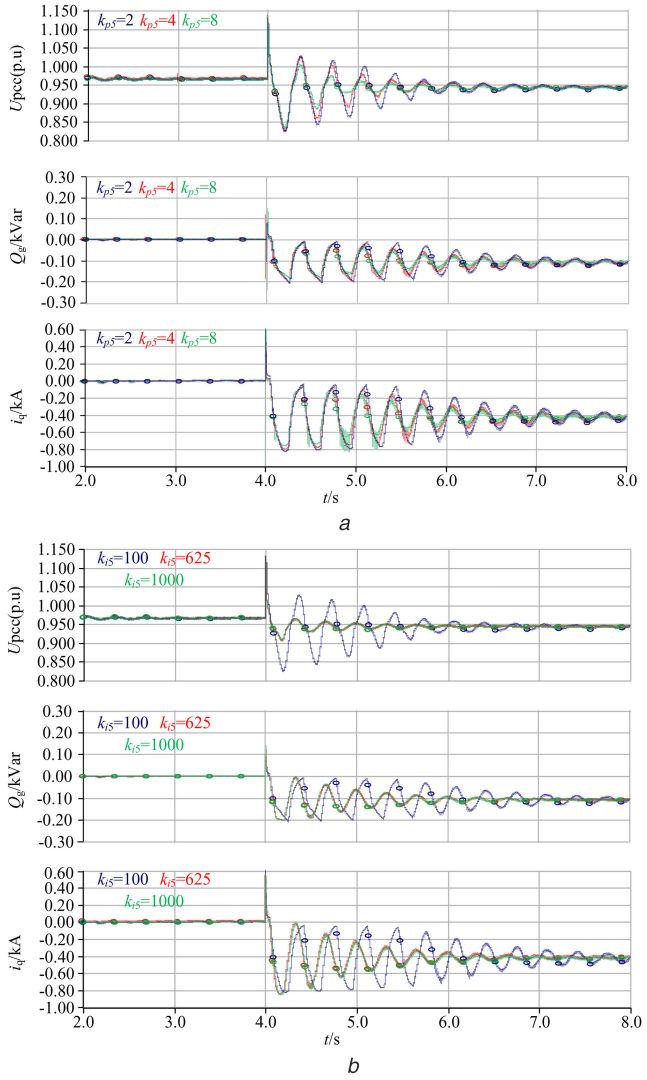


**Fig. 12**

***(a)*** Response speed of different reactive loop different proportional coefficient $k_{p5}$, ***(b)*** Response speed of different reactive loop different integral coefficient $k_{i5}$

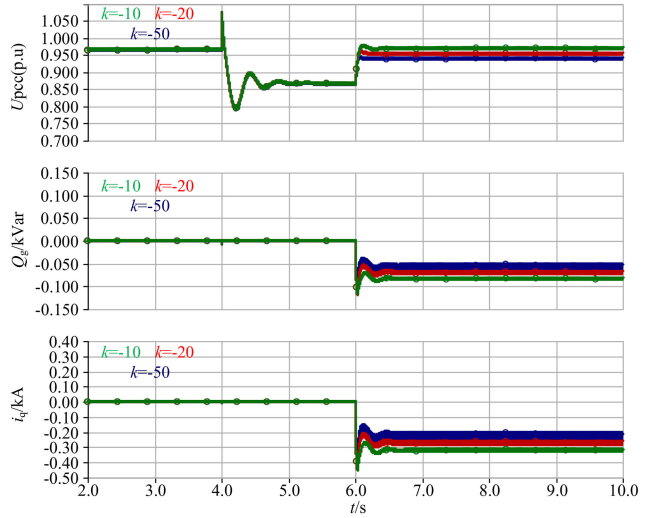


**Fig. 13** *Reactive power compensation ability of different k*

### *5.2 Simulation of different adapted control coefficient*

Figs. 13 and 14 show the PCC voltage $U_{PCC}$, rated DC voltage $U_{DC}$, $q$-axis component current $i_q$ and output reactive power $Q_g$ when SCR = 4, $k_{p5}$ = 2, $k_{i5}$ = 100 at different values of $k$.

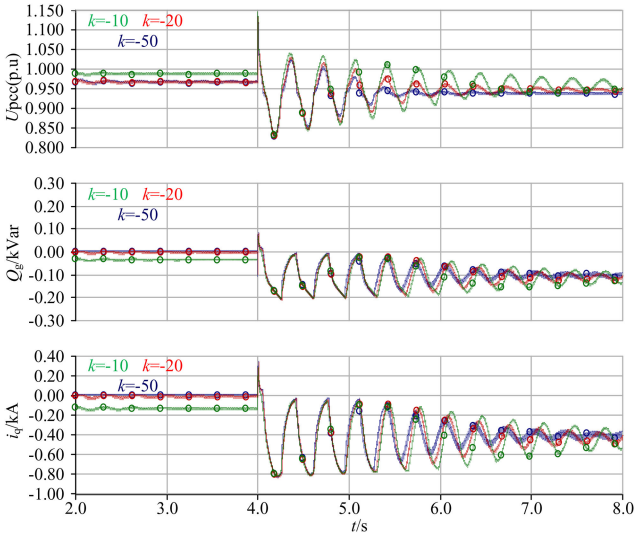


**Fig. 14** *Response speed of different k*

The total time of simulation is 12 s. The green, red and blue lines indicate that value of reactive power control parameter $k$ are −10, −20 and −50. When $t$ = 4 s, the increasing of grid impedance makes PCC voltage drop. When $t$ = 6 s, reactive voltage control plays a role in increasing PCC voltage. From Fig. 10, it is not hard to see that proposed control method through the real-time detection PCC voltage, automatically obtain the reactive demand to maintain PCC voltage by PI controller and realises the dynamic adjustment, maintains PCC voltage within an acceptable range. As the absolute value of reactive power control parameter $k$ increase, the better reactive power compensation ability of the method is.

The total time of simulation is 8 s. When $t$ = 4 s, the increasing of grid impedance makes PCC voltage drop, reactive power control is thrown into system directly. Different $k$ are used to determine response speeds under the same grid disturbance. From Fig. 14, the larger absolute value corresponds to the faster response speed.

## 6 Conclusion

In this paper, a simple and effective adapted Reactive Power Control strategy has been proposed and validated using PSCAD/EMTDC simulations. It shows that the method utilises all the available capacity of VSC (when it is needed) without violating maximum capacity limitation, and provides reactive power support for the system. A small-signal model for PV generation is established to investigate its stability with varies grid strength, reactive loop parameters, and reactive power parameters. The following conclusions are obtained:

i. With the decrease of grid strength, the stability of the small-signal model becomes worse.
ii. With the increase of the absolute value of reactive power control parameters, the small-signal stability becomes better.
iii. Increasing of reactive loop parameters makes the small-signal stability better, but not obviously.
iv. With the same grid disturbance, the larger absolute value of $k$ represents the better of the VSC performance to meet the reactive power demand and the faster response speed.

## 7 Acknowledgments

This work is supported by Research Program of State Grid Corporation of China (study on active frequency and voltage control technologies for second level power disturbance in photovoltaic power plant).

## 8 References

[1] Komoto, K., Ehara, T., Xu, H., *et al.*: '*Energy from the desert: very large scale PV power plants for shifting to renewable energy future*' (International Energy Agency, Paris, France, 2015)

[2] Brown, T.: 'Transmission network loading in Europe with high shares of renewables', *IET Renew. Power Gener.*, 2015, **9**, (1), pp. 57–65
[3] Hu, J.B., Huang, Y.H., Wang, D., *et al.*: 'Modeling of grid-connected DFIG-based wind turbines for DC-link voltage control stability analysis', *IEEE Trans. Sust. Energy*, 2015, **6**, pp. 1325–1336
[4] Ge, H., Bi, R., Xu, Z.C., *et al.*: 'Research on reactive power and voltage control of large-scale photovoltaic power station', *Power Syst. Prot. Control*, 2014, (14), pp. 45–51
[5] Liu, Y, Bebic, J, Kroposki, B, *et al.*: 'Distribution system voltage performance analysis for high penetration PV'. IEEE Energy 2030 Conf., Atlanta, GA, 2008, pp. 1–8
[6] Alam, M, Muttaqi, K, Sutanto, D.: 'A multi-mode control strategy for var support by solar PV inverters in distribution networks', *IEEE Trans. Power Syst.*, 2015, **30**, (3), pp. 1316–1327
[7] Jahangiri, P, Aliprantis, D.: 'Distributed volt/var control by PV inverters', *IEEE Trans. Power Syst.*, 2013, **28**, (3), pp. 3429–3439
[8] Zhang, W., Liu, Z.M., Shen, L.X.: 'Flexible grid-connection of photovoltaic power generation system with energy storage system for fluctuation smoothing', *Electr. Power Autom. Equip.*, 2013, **33**, (5), pp. 106–111